Study of Ni catalysts on different supports to obtain synthesis gas

Francisco Pompeo[a, b], Nora N. Nichio[a, b], Osmar A. Ferretti[a, b, *], Daniel Resasco[c]

[a]*CINDECA, Fac. Ciencias Exactas, UNLP -CONICET, 47 N°257, 1900 La Plata, Argentina*
[b]*Fac. Ingeniería, Universidad Nacional de La Plata, 1 Esq. 47, (1900) La Plata, Argentina*
[c]*School of Chemical Engineering and Materials Science, University of Oklahoma, 100 E. Boyd Street, Norman, OK 73019, USA*

Abstract

Ni catalysts supported on α-Al_2O_3, ZrO_2 and α-Al_2O_3–ZrO_2 were studied in the synthesis gas reactions (partial oxidation, dry reforming and mixed reforming). The Ni/α-Al_2O_3–ZrO_2 catalyst showed a very good performance in relation to the initial activity and selectivity, comparable to that of the Ni/α-Al_2O_3 catalyst. Concerning the deactivation, the modification of the α-Al_2O_3 supported with ZrO_2 leads to a higher stability, due to the strong inhibition of the carbon formation during the reaction. These results suggest that ZrO_2 promotes the gasification of adsorbed intermediates, which are precursors of carbon formation. Temperature programmed oxidation, transmission electron microscopy and Raman spectroscopy experiments showed that on Ni/α-Al_2O_3 catalyst high amounts of graphitic carbon (whisker-like) are deposited during CO_2 reforming reaction, while on Ni/α-Al_2O_3–ZrO_2 lesser amounts of deposited carbon were observed (about one order lower); a fraction of this carbon is of the same nature as that observed on Ni/α-Al_2O_3 catalyst, while the other fraction is composed of carbon nanotubes, both of single wall and multi wall.

1. Introduction

The production of hydrogen (and/or *syngas*) is gaining importance during the last years due to its use as clean energy source in fuel cells and eventually in automobiles, which has led to the denomination of "the fuel of future". In addition to the projected new demands, existing demands in refineries are also growing due to the increase in severity of the hydro-treatments required to fulfill the stricter environmental legislation. The synthesis gas is feedstock of a number of processes such as ammonia plants (fertilizers), Fischer–Tropsch processes to produce diesel fuels and synthetic gasolines, and methanol synthesis plants, which finds diverse uses in the energy sector (methanol fuel cells, energetic vector, MTG, MTBE) [1]. Commercially, synthesis gas is produced almost exclusively via reforming of natural gas with steam, but this process has drawbacks associated with its high energy cost (reaction highly endothermic and operation at high water/methane volumes). Alternative routes such as partial oxidation of methane (POM), dry reforming (DR) with CO_2, and the mixed reforming (MR) with O_2, CO_2 and/or H_2O appear as attractive alternatives [2].

Transition metals (Ni, Pt, Rh, Ru) have been shown to exhibit a good level of activity and selectivity for all three reactions, POM, DR and MR [3]. The main problem that is typically encountered using these catalysts is due to deactivation by carbon deposition and sintering. The deactivation phenomena are particularly severe in these processes due to the harsh conditions at which they are conducted, low H/C and O/C ratios and high temperatures. For all of

these, α-Al$_2$O$_3$ is a suitable support due to its chemical and physical stability as well as its high mechanical resistance. However, the weak interaction with the precursors of the active species results in a poor sintering tolerance [4]. Consequently, the development of active, selective, and mechanically and chemically stable catalytic systems is a desirable goal for the effective production of hydrogen (and/or *syngas*) in alternative processes to conventional steam reforming.

In previous work, it has been demonstrated that ZrO$_2$ has interesting properties as a catalyst modifier [5,6]. For example, it has been used in the case of Pt supported on γ-Al$_2$O$_3$, improving the catalyst stability [7]. In the present contribution, catalysts based on Ni supported on α-Al$_2$O$_3$ have been modified by the addition of ZrO$_2$ for the production of synthesis gas via POM, DR and MR reactions. The objective of the study is to investigate the effects of ZrO$_2$ addition on the catalytic properties of supported Ni, particularly its stability.

2. Experimental

Catalysts based on Ni were prepared using several supports, ZrO$_2$ (NiZ), α-Al$_2$O$_3$(NiA), and α-Al$_2$O$_3$ modified by impregnation of 1% ZrO$_2$ (NiAZ). The ZrO$_2$ support had a BET surface area of 62 m^2 g^{-1}. The α-Al$_2$O$_3$ support obtained from Rhone Poulenc had a surface area of 10 m^2 g^{-1}. The α-Al$_2$O$_3$–ZrO$_2$ support (1% in ZrO$_2$) was the same alumina modified by impregnation with a solution of zirconium hydroxide in HNO$_3$ (50 vol%) and subsequently calcined in air (16 h at 550 °C).

The Ni catalysts were prepared by impregnation of supports previously calcined at 500 °C for 2 h with nickel nitrate in aqueous medium, with the appropriate concentration to obtain a Ni content of 2% in weight in the final solid.

Temperature programmed reduction (TPR) was carried out in a conventional dynamic equipment using a H$_2$/Ar ratio of 1/9 and a heating rate of 10 °C min^{-1} from room temperature to 1000 °C.

The experimental equipment utilized for catalytic tests is described in Ref. [2]. The activity and selectivity of the catalysts were determined at atmospheric pressure, feed flow of 130 cm^{3}min^{-1}, reaction temperatures in the range of 600–750 °C, composition of the feed mixture for POM: N$_2$/CH$_4$/O$_2$ = 10/2/1, for DR: N$_2$/CH$_4$/CO$_2$ = 6/1/1 and for MR: N$_2$/CH$_4$/O$_2$/CO$_2$ = 22/4/2/1 (the partial pressure of methane was similar for all reactions). The catalyst weight was 0.025 g and the grain size between 0.12 and 0.15 mm. The stability test was carried out at constant temperature (700 °C), for 50 h. The stability was evaluated in terms of the activity coefficient aCH$_4$, which represents the ratio between the consumption rate of CH$_4$ at time t hours in reaction and the initial consumption rate. The feed flow composition and the products of the reaction were analyzed with a Shimadzu GC-8A gas chromatograph, connected on line to the reactor apparatus via gas sampling valve. Separation of H$_2$, O$_2$, CH$_4$ and CO occurred on a column containing

5A Molecular Sieve, whereas separation of CO$_2$ occurred on a column containing Porapak Q, at 313 K. Carbon deposits produced during stability tests were characterized by temperature programmed oxidation (TPO), measuring the weight variation as a function of the temperature in a thermogravimetric equipment (Shimadzu TGA50). Post-reaction samples of 0.015 g were used feeding with air at flow of 10 cm^{3}min^{-1} and a heating program of 10 °C min^{-1} from room temperature up to 850 °C.

Transmission electron microscopy (TEM) images were taken by means of a TEM JEOL FX 2000, operated at 200 KV. A graphite pattern was used for calibration. In this analysis, a suspension in 2-propanol was prepared by stirring the solid sample with ultrasound for 10 min. A few drops of the resulting suspension were deposited on a TEM Cu grid (Lacey carbon film 300 mesh, electron microscopy science) and subsequently dried and evacuated before the analysis. To estimate the average particle size (d_{TEM}), the particles were considered spherical and the diameter volume–area was calculated by using expression (1):

$$d_{TEM} = \frac{\sum n_i \cdot d_i^3}{\sum n_i \cdot d_i^2}, \tag{1}$$

where n_i is the number of particles with diameter d_i.

Raman spectra were obtained in a Jovin Yvon–Horiba Lab Ram 800 equipped with a coupled device detector (CCD) and with a laser excitation source whose wavelength is 633 nm (He–Ne Laser).

3. Results and discussion

With respect to the supports used for the catalysts, the XRD diagrams, the specific surface area and pore volume of the α-Al$_2$O$_3$–ZrO$_2$ (AZ) support did not differ from what was obtained for the α-Al$_2$O$_3$ (A), which indicates that with this Zr content (1% in ZrO$_2$), the morphological, textural, and structural properties of α-Al$_2$O$_3$ remain unaffected.

Table 1 summarizes the characteristics of the catalytic systems studied in this work. After the Ni impregnation process, no appreciable change in BET surface was observed.

Results of particle size distribution from TEM are presented as histograms in Fig. 1. These histograms indicate a more homogeneous size distribution for the catalytic systems supported on ZrO$_2$ (NiZ) and α-Al$_2$O$_3$–ZrO$_2$ (NiAZ) than for the NiA catalyst, for which a high concentration of particles around 17 nm was observed coexisting with a considerably smaller group of particles about 28 nm. For the NiAZ system, the distribution is clearly unimodal and centered in about 14 nm, while for the NiZ catalyst, the distribution is also unimodal and centered around 4 nm. These TEM results can be used to estimate metal dispersion values [8] (calculated as $D\% = 97/d_{TEM}$, d_{TEM} in nm). Accordingly, the metal dispersions would be 5.4% and 6.9% for NiA and NiAZ, respectively, which is in agreement with results

Table 1
Characterization of the studied catalysts

Catalysts	S_{BET} (m^2 g^{-1})	Ni (w/w%)	D (%)	d_{TEM} (nm)	TPR	
					Main peak (°C)	Secondary peak (°C)
NiA	10	2	5.4	17–28	552	460–584–680
NiAZ	10	2	6.9	14	530	460–555–628
NiZ	60	2	19.4	5	445	390

BET surface areas, Ni dispersions (D), mean particle size (d_{TEM}) and temperature programmed reduction (TPR).
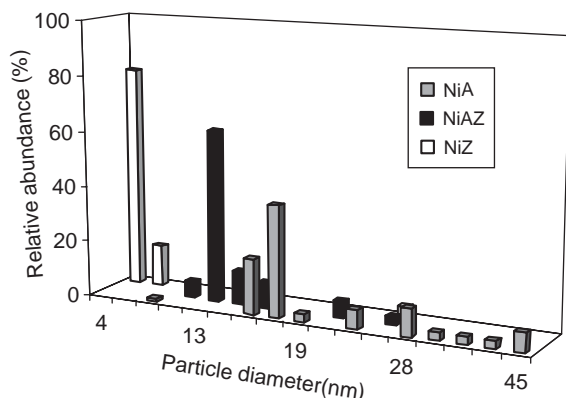

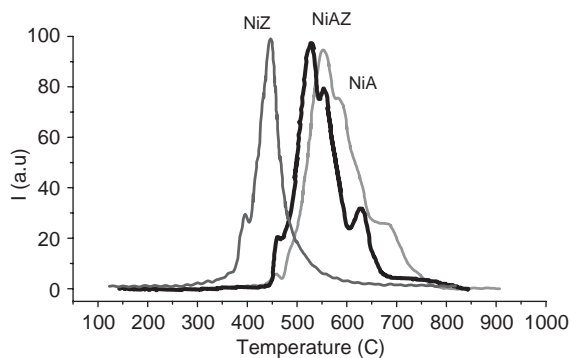Fig. 1. Particle size distribution for the fresh catalysts (TEM).

Fig. 2. Temperature programmed reduction TPR profiles for NiZ, NiAZ and NiA catalysts. For the conditions, see the text.

previously reported for Ni/α-Al$_2$O$_3$ systems [4,9]. In the case of the NiZ system, the estimated dispersion is 20%.

Results obtained by TPR (Table 1 and Fig. 2) show reduction peaks for all samples between 400 and 700 °C, which are typical of supported nickel species [10]. The NiA catalyst exhibited its principal reduction peak at 552 °C, the NiAZ at 530 °C and the NiZ at 445 °C. It is well known that on NiA catalysts, Ni species may be present forming mixed oxides

Table 2
Methane conversion, H$_2$/CO ratio and yield of CO (Yield CO (%) = [CO$_{out}$/(CO$_{2in}$ + CH$_{4in}$)]) at 2 h of reaction (POM, DR, MR) for the studied catalysts (for the conditions), see the text

Catalysts	Reaction	Temp. (°C)	XCH$_4$ (%)	Yield CO (%)	H$_2$/CO
NiA	DR	600	20	14	0.9
		650	30	23	1.1
		700	44	33	1.1
	POM	600	56	35	2.9
		650	65	46	2.6
		700	77	56	2.5
	MR	600	36	32	1.8
		650	48	47	1.7
		700	60	60	1.6
NiAZ	DR	600	30	22	1.1
		650	42	33	1.1
		700	54	43	1.1
	POM	600	49	28	2.7
		650	55	36	2.4
		700	62	47	2.2
	MR	600	38	27	1.7
		650	48	40	1.6
		700	57	50	1.6
NiZ	DR	600	14	7	1.1
		650	22	14	1.1
		700	36	27	0.9
	POM	600	24	2	3.2
		650	39	17	2.7
		700	46	26	2.3
	MR	600	15	4	1.4
		650	24	14	1.4
		700	38	30	1.5

of Ni and Al, which can be described as surface spinel-type structures [10,11]. The catalyst supported on ZrO$_2$ shows reduction temperatures markedly lower compared with catalysts supported on α-Al$_2$O$_3$. In the case of the system supported on α-Al$_2$O$_3$ modified by ZrO$_2$, the principal peak of hydrogen consumption is found among the ones observed for NiA and NiZ. This behavior is explained by the presence of ZrO$_2$ that modifies the original support hindering the interaction between nickel and alumina, which explains the shift from 552 to 530 °C, for NiA and NiAZ, respectively. Another evidence of the specific interaction between the Ni and the ZrO$_2$ is a slight growth of the peak at 445 °C, when going from NiA to NiAZ; this peak is ascribed to Ni on ZrO$_2$, being coincident with the principal peak observed in the NiZ system.

Table 2 summarizes the results corresponding to catalytic activity, yield to CO, and H$_2$/CO ratio obtained on the POM, DR and MR reactions by using NiA, NiAZ and NiZ catalysts. These results show high activity values, following the

sequence POM > MR > DR. For the POM reaction, two different reaction mechanisms have been previously proposed, direct partial oxidation (one-step mechanism) or total oxidation of a part of methane and subsequent reforming of the remaining methane (two-steps mechanism). These results are in agreement with our previous works [2,9] that indicate the coexistence of both mechanisms, in which according to Qin et al. [12], the contribution of each mechanism depends on the relation between the gaseous oxygen concentration and the adsorbed atomic oxygen concentration. The lower reaction rate in a MR would be due to a lower contribution of the direct partial oxidation.

The H_2/CO ratio is a very important property in the reforming processes since different H_2/CO values are required according to the process that utilizes the synthesis gas. In this study, the observed H_2/CO values show a small dependence on the catalyst being used. For the DR and POM reactions, at 700 °C, they are near to the stoichiometric value, next to 1 and 2, respectively. For the MR reaction, the H_2/CO ratio varies between 1 and 2, which suggests that this reaction could be used to control such ratio, and in addition to the advantages related to the possibility of reaching autothermic conditions.

With respect to the DR reaction, higher values of activity and yield to CO (Y_{CO}%) are observed for the NiAZ catalyst than for the NiA catalyst. It appears that ZrO_2, modifying the α-Al_2O_3 and interacting with Ni active phase, is able to enhance the CO_2 activation. It is well known that alpha alumina is neither able to activate methane nor CO_2; while in the bibliography, it has been reported that the ZrO_2 is able to activate the CO_2 in the M/ZrO_2 (M: Pt, Ni) interface [13–15]. For Pt/ZrO_2 catalyst, results reported in Ref. [16] have been explained via two independent paths. The first path would involve the decomposition of CH_4 on the metal particle, resulting in the formation of H_2 and carbon, which could partially reduce the oxide support near the metal particle or, in the absence of a reducible oxide, could form carbon deposits on the metal. The second path would be the dissociation of CO_2 to form CO and O. The oxygen formed during the dissociation could then reoxidize the support to provide a redox mechanism for continuous cleaning. The balance between the rates of decomposition and cleaning would determine the overall stability of the catalyst.

For the POM reaction, the activity of NiAZ catalyst is lower than that of NiA. New investigations are necessary in order to elucidate interactions between oxygen and the Ni–ZrO_2 phase and to explain this lower activity observed on NiAZ. We can speculate that the presence of ZrO_2 modifies the nature and/or availability of the oxygen that participates in the direct POM to synthesis gas, as proposed in the literature [14,15]. So, a smaller contribution of the direct partial oxidation in relation to the two-step mechanism could explain these results. For the MR reaction, our results confirm the effect of gaseous O_2; in this case, the amount of O_2 is lower than for POM and consequently the negative effect of activity for NiAZ is also less pronounced.
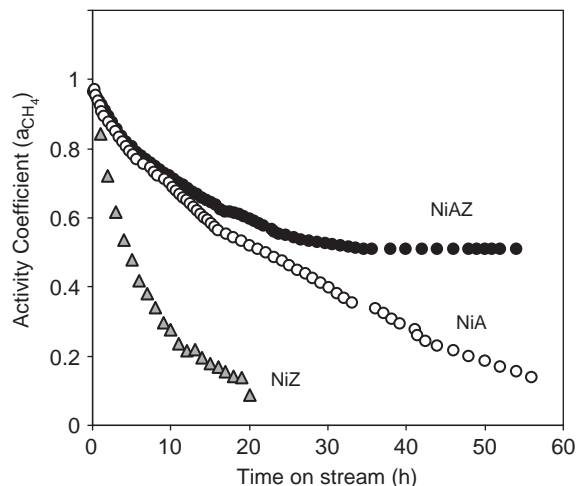

Fig. 3. Deactivation tests of the studied catalysts at 700 °C (NiA (○), NiAZ (●), NiZ (▲)). For the conditions, see the text.

Concerning the NiZ catalyst, in spite of the higher Ni dispersion than on NiA and NiAZ, the activity is lower for all the reactions investigated. In addition, NiZ is seen to deactivate very quickly, as shown in Fig. 3. Previous results reported in the literature have shown that the stability of Ni/ZrO_2, in DR reactions, is strongly dependent on the preparation method of the support precursor; when ZrO_2 supports are prepared from conventional procedures, catalysts deactivate as rapidly as seen in our NiZ sample [15].

As mentioned in the introduction, the stability of the active phase is a property as important as the activity and selectivity for the different production processes of synthesis gas from methane. For this reason, the stability of the catalysts was analyzed for the DR process as it can be seen in Table 2. As reported in previous studies, the DR process is the one with most severely deactivating conditions [2,17]. Fig. 3 shows the results of the activity as a function of reaction time for DR, noting that the NiA catalyst suffers a deactivation more pronounced than the NiAZ; activity coefficients after 48 h reaction are 0.24 and 0.51, for NiA and NiAZ, respectively.

Micrographs obtained by TEM on post-reaction NiA and NiAZ catalysts showed a distribution of particle sizes similar to the ones of the fresh catalysts. It is reasonable to conclude that, for our operating conditions, sintering does not contribute in an important way to the deactivation phenomenon. On the other hand, on this NiA catalyst, micrographs of Fig. 4 evidence a high concentration of carbon deposits, while a much lesser amount is observed in the NiAZ catalyst. These notable differences are even more clearly evident in the TPO profiles shown in Fig. 5. The amount of carbon deposited on each catalyst as determined by thermogravimetry was almost an order of magnitude higher difference on the NiA catalyst (6.9 wt% C) in comparison to the amount of carbon on the NiAZ system (0.9 wt% C).

Fig. 5. Temperature-programmed oxidation (TPO) of carbon species formed after DR deactivation test at 700 °C. NiA (----) and NiAZ (—).
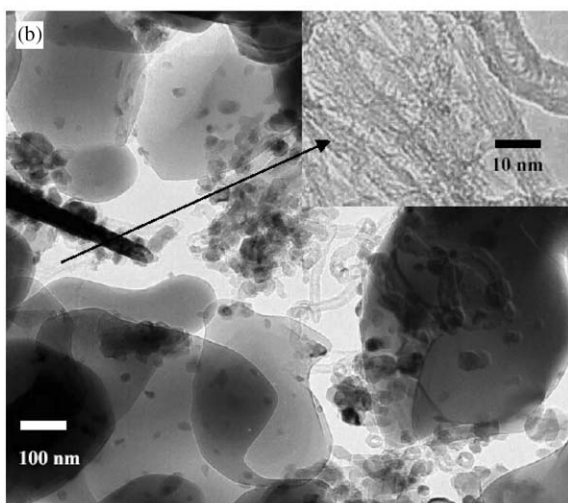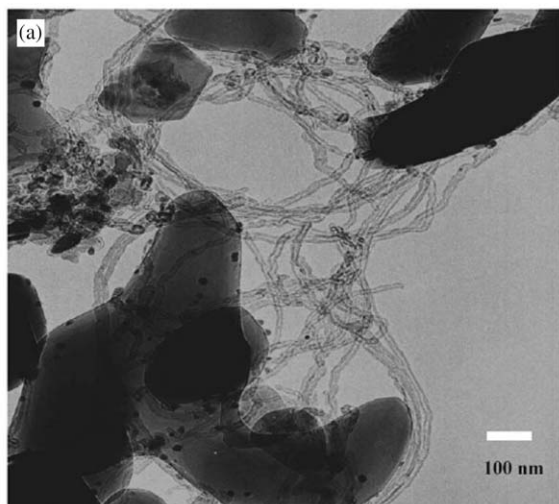

Fig. 4. (a) TEM micrographs of NiA catalyst, after DR deactivation test at 700 °C. (b) TEM micrographs of NiAZ catalyst, after DR deactivation test at 700 °C.The inner figure shows the formation of Single Walled Carbon Nanotubes.

A well-known fact is that Ni can dissolve carbon and generate carbon filaments [3]. During this process, metallic sites remain uncovered despite the deposition of large amounts of carbon, thus resulting in much lower deactivation rates than those expected if metal-covering coke deposits occurred [18]; for example, in the case of NiA (2 wt% Ni, $D = 5.4\%$), the activity coefficient is 0.24 although the carbon deposition (6.9 wt% C) represents a C/Ni^{sup} ratio of 312. However, even taking into account this characteristic form of carbon deposition, a simple comparison of NiA and NiAZ catalysts shows that there is a relationship between the carbon content and the deactivation level.
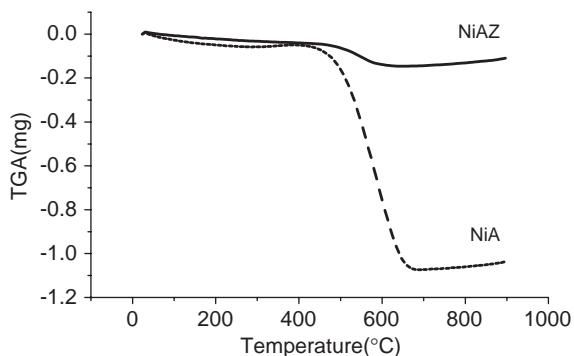
In any case, even if all the Ni remains exposed at the top of the carbon filament without presenting immediate deactivation, the growth of these filaments causes the rupture of the catalyst grain, which makes improbable the industrial use of systems operating under these conditions.

It is evident that the carbon formation is a regulating factor for the stability of the active phase and that the presence of ZrO_2 plays a fundamental role in minimizing this process. In the NiAZ system, the characterization results allow us to conclude that Ni is deposited in intimate contact with the ZrO_2 that modifies the α-Al_2O_3 support. It can be proposed that the CO_2 adsorbs dissociatively on the boundary between ZrO_2 and Ni, favoring the gasification of intermediates strongly unsaturated, precursors of carbon deposits and thus avoiding the formation of characteristic filaments in these systems. Similarly, on Pt/γ-Al_2O_3 and Pt/γ-Al_2O_3–ZrO_2 catalysts, the higher stability and activity to *syngas* has been reported in the ZrO_2-containing catalyst was attributed to an increase in the dissociative chemisorption capacity of CO_2 on the Pt–ZrO_2 interface [7].

From the TEM micrographs shown in Fig. 4 it can be observed that in the case of the NiA catalyst, carbonaceous deposits are filamentous in nature (*whiskers*). These deposits appear preferentially on metal particles of larger size, which is in agreement with what was reported by Demicheli et al. [19] for Ni supported on θ-Al_2O_3–CaO. In the case of the NiAZ catalyst, the concentration of carbonaceous deposits is notably lower, in agreement with the TPO results and the stability tests mentioned above. In this case, the incipient amounts of carbon deposits exhibit two types of structures, one similar to the one observed for NiA and the other of the type so-called single wall carbon nanotubes (SWNT) [20,21].

The analysis by Raman spectroscopy of post-reaction samples confirms the existence of two types of carbon structures for the case of NiAZ catalyst. Fig. 6 shows the Raman spectra recorded on both catalysts after the stability test.
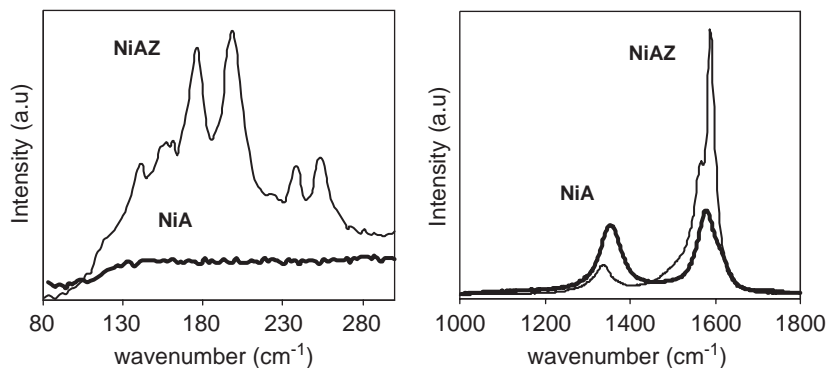
Fig. 6. Raman spectra of carbon species formed after DR deactivation test at 700 °C.

The tangential mode G band appearing in the 1500–1700 cm^{-1} region is related to the Raman-allowed phonon mode E_{2g} and involves out-of-phase intra-layer displacement in the graphene structure. It provides information about the electronic properties of the filamentous carbons and is a measure of the presence of ordered carbon. Comparing this G bands to that of original graphite at 1581 cm^{-1}, we conclude that peaks are due to the presence of graphitic carbon in these solids. Additionally, a band at about 1350 cm^{-1} so-called D band was observed for both catalysts. Because D band is associated with defective and disordered structures, we may conclude that they are carbon nanoparticles, amorphous carbon, or defective filamentous carbon. Hence, the size of the D band relative to the G band can be used as a qualitative measurement for the formation of different kinds of carbon [22]. Finally, a band around 200 cm^{-1}, corresponding to the radial breathing mode (A_{1g}, E_{1g}, E_{2g} bands) provides evidence for the presence of SWNT in the NiAZ catalysts. These results are in concordance with the TEM and TPO analysis.

The characterization of carbon deposits by Raman, TEM and TPO complement the results of the catalytic tests. Thus, it is established that the ZrO_2 layer modifying the base support of α-Al_2O_3 leads to a Ni deposit with a specific Ni–ZrO_2 interaction. This system (NiAZ) exhibits specific catalytic properties with respect to carbon deposition, leading to catalysts with a higher stability "on stream".

4. Conclusions

Catalytic systems based on Ni supported on alpha alumina modified by ZrO_2 have been prepared, achieving a specific interaction between the Ni and the modified support that results in very good catalytic properties with respect to the methane transformation to *syngas*.

The Ni catalysts supported on α-Al_2O_3 modified by ZrO_2 present a very good level of activity and selectivity. In addition, these systems are more stable than those corresponding to unmodified Ni supported on α-Al_2O_3 and this stability enhancement can be associated to a lower rate of carbon formation.

It is suggested that the ZrO_2 additive, due to its capacity for the activated adsorption of CO_2, promotes higher levels of activity for the DR reaction and the gasification of intermediate precursors in the carbon generation. It was determined that the nature of the carbon deposits is a function of the support. On the Ni/α-Al_2O_3 catalysts high carbon contents of the filamentous type (*whisker*) are obtained. By contrast, on the Ni/α-Al_2O_3–ZrO_2 formation of smaller deposits containing graphitic carbon and carbon nanotubes (SWNT) have been observed.

References

[1] Peña MA, Gómez JP, Fierro JLG. New catalytic routes for syngas and hydrogen production. Appl Catal A 1996;144: 7–57.

[2] Nichio NN, Casella ML, Santori GF, Ponzi EN, Ferretti OA. Stability promotion of Ni/α-Al_2O_3 catalysts by tin added via surface organometallic chemistry on metals, Applications in methane reforming processes. Catal Today 2000;62:231–40.

[3] Rostrup-Nielsen JR, Hansen JH. Carbon dioxide reforming of methane over transition metals. J Catal 1993;144:38–49.

[4] Casella ML, Nichio NN, González ML, Ferretti OA. Study of different support and precursor compounds for supported nickel oxyreforming catalysts. Mater Lett 1998;37:290–3.

[5] Lercher JA, Bitter JH, Hally W, Niessen W, Seshan K. Design of stable catalysts for methane carbon dioxide reforming. Stud Surf Sci Catal 1996;101:463–72.

[6] Sheng W, Jun KW, Roh HS, Liu ZW, Park SE. Comparative study on partial oxidation of methane over Ni/ZrO_2, Ni/CeO_2 and $Ni/Ce–ZrO_2$ catalysts. Catal Lett 2002;78:215–22.

[7] Souza M, Aranda D, Schmal M. Reforming of methane with carbon dioxide over $Pt/ZrO_2/Al_2O_3$ catalysts. J Catal 2001;204:498–511.

[8] Farrauto RJ, Bartholomew CH. Fundamentals of industrial catalytic processes. London: Blackie Academic & Professional; Chapman & Hall; 1997. p. 81.

[9] Nichio NN, Casella ML, Ponzi EN, Ferretti OA. Ni/Al_2O_3 catalysts for syngas obtention via reforming with O_2 and/or CO_2. Stud Surf Sci Catal 1998;119:723–8.

[10] Molina R, Poncelet G. α-Alumina-supported nickel catalysts prepared from nickel acetylacetonate: a TPR study. J Catal 1998;173:257–67.

[11] Villacampa JL, Royo C, Romeo E, Montoya A, Del Angel P, Monzon A. Catalytic decomposition of methane over Ni/Al_2O_3 coprecipitated catalysts reaction and regeneration studies. Appl Catal A 2003;252:363–83.

[12] Qin D, Lapszewicz J, Jiang X. Comparison of partial oxidation and steam-CO_2 mixed reforming of CH_4 to syngas on MgO-supported metals. J Catal 1996;159:140–9.

[13] Stagg-Williams SM, Noronha FB, Fendley G, Resasco DE. Carbon dioxide reforming of CH_4 over Pt/ZrO_2 catalysts promoted with La and Ce oxides. J Catal 2000;194:240–9.

[14] Xu BQ, Wei JM, Yu YT, Li JL, Zhu QM. Carbon dioxide reforming of methane over nanocomposite Ni/ZrO_2 catalysts. Top Catal 2003;22:77–85.

[15] Wei JM, Xu BQ, Li JL, Cheng ZX, Zhu QM. Highly active and stable Ni/ZrO_2 catalyst for syngas production by CO_2 reforming of methane. Appl Catal A: Gen 2000;196:L167–72.

[16] Stagg SM, Romeo E, Padro C, Resasco DE. Effect of promotion with Sn on supported Pt catalysts for CO_2 reforming of CH_4. J Catal 1998;178:137–45.

[17] Hou Z, Yokota O, Tanaka T, Yashima T. Characterization of Ca-promoted $Ni/α-Al_2O_3$ catalyst for CH_4 reforming with CO_2. Appl Catal A 2003;253:381–7.

[18] Nichio NN, Casella ML, Ferretti OA. Influence of the support and precursor compounds on the stability of supported nickel oxyreforming catalysts. React Kinet Catal Lett 1999;66: 27–32.

[19] Demicheli MC, Duprez D, Barbier J, Ponzi EN, Ferretti OA. Deactivation of steam-reforming model catalysts by coke formation. II. Promotion of K and effect of water. J Catal 1994;145:437–60.

[20] Saito R, Fujita M, Dresselhaus G, Dresselhaus MS. Electronic structure of graphene tubules based on C_{60}. Phys Rev B 1998;57(7):4145–9.

[21] Saito R, Takeya T, Kimura T, Dresselhaus G, Dresselhaus MS. Raman intensity of single-wall carbon nanotubes. Phys Rev B 1992;46(3):1804–11.

[22] Alvarez WE, Pompeo F, Herrera JE, Balzano L, Resasco DE. Characterization of single-walled carbon nanotubes (SWNTs) produced by CO disproportionation on Co–Mo catalysts. Chem Mater 2002;14:1853–8.